Faraday Discussions

Ionic current driven by a viscosity gradient

Journal:	*Faraday Discussions*
Manuscript ID	FD-ART-02-2023-000053.R1
Article Type:	Paper
Date Submitted by the Author:	18-May-2023
Complete List of Authors:	Wiener, Benjamin; Brown University, Physics Department Stein, Derek; Brown University, Physics Department

SCHOLARONE™
Manuscripts

Journal Name

ARTICLE TYPE

Cite this: DOI: 00.0000/xxxxxxxxxx

Ionic current driven by a viscosity gradient†

Benjamin Wiener[a] and Derek Stein*[a]

Received Date
Accepted Date

DOI: 00.0000/xxxxxxxxxx

Gradients of voltage, pressure, temperature, and salinity can transport objects in micro- and nanofluidic systems by well known mechanisms. This paper explores the dynamics of particles in a viscosity gradient with numerical simulations. The different stochastic rules used to integrate the random motion of Brownian particles affect the steady-state distribution of particles in a diffusivity gradient. Importantly, the simulations illuminate the important role that the boundary conditions play, disallowing a steady-state flux when the boundary conditions mimic those of a closed container, but allowing flux when they mimic electrodes. These results provide a possible interpretation for a recent series of measurements in which a steady ionic current flowed between electrodes separated by a nanofluidic channel with a liquid viscosity gradient.

1 Introduction

In experimental work to be reported elsewhere, we studied ionic transport inside nanofluidic devices in which we set up a controlled viscosity gradient by pumping fluids of known viscosity past either end of a channel with no applied voltage, pressure, or salinity gradient. Currents on the order of 10 to 100 pA flowed in the direction of lower viscosity through the 200 μm-long and 150 μm-wide channels filled with liquids with viscosities that varied from 1 to 5 mPa s. The nanofluidic devices enabled a thorough characterization of the current's dependence on experimental parameters like the viscosities of the liquids, the length of the channel, the surface charge density, and the bulk salinity. The currents increased linearly with the gradient of the inverse viscosity and the channel's surface charge density but were insensitive to the bulk salinity. These findings point to the counterions in the Debye screening layer of a channel's inner surface as the carriers of the ionic currents and the viscosity gradient as the source of the counterions' net motion. Here, we theoretically investigate whether a steady ionic current can be explained by the Brownian motion of counterions in a viscosity gradient.

Einstein famously showed that the Brownian motion of an object is fundamentally linked to its viscous drag in a fluid because the same atomic-scale bumps that cause Brownian motion also randomize the motion of a drifting particle and eventually bring it to rest[1,2]. It is not possible to know the details of the atomic scale bumps, but one can model a Brownian motion as a string of stochastic processes that resembles a random walk[3,4]. The stochastic step size is positively related to the diffusivity, D, which is inversely related to the viscosity, η.

The mathematician Kiyosi Itô invented a method for integrating stochastic processes[5,6]. He generalized the Riemann-Stieltjes integral, whereby one divides a function into tiny intervals and sums the area under the curve based on the value of the function in each interval. A smooth function can be sampled anywhere within the interval because the possible choices all converge to the same value in the limit of small intervals. However, a Brownian motion is not smooth on any scale, and no matter how small the interval, the integral depends on the arbitrary choice of where within each interval one evaluates the function. Itô's convention is to evaluate the function at the beginning of each interval[5]. Ruslan Stratonovich[7,8], Donald Fisk[9], and Peter Hänggi[10,11] later developed alternatives to Itô's integral, each giving a different but completely self-consistent formulation of stochastic calculus. The Stratonovich (–Fisk) integral evaluates the function in the middle of each interval and preserves the chain rule of ordinary calculus, while the Hänggi (or isothermal) integral evaluates the function at the end of each interval.

The differences between the integration conventions are

[a] Physics Department, Brown University, Providence, RI, USA.
* E-mail: derek_stein@brown.edu

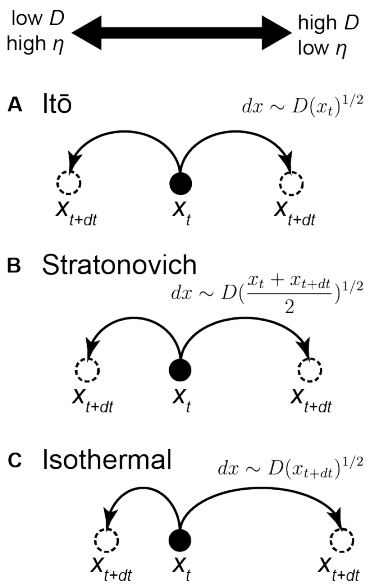

Fig. 1 Stochastic displacement models. Illustrations show leftward and rightward steps of random walks corresponding to (a) the Itô, (b) the Stratonovich rule, and (c) the isothermal rule.

physically meaningful in the case of a Brownian particle moving in a liquid viscosity gradient because that particle's stochastic step size depends on the viscosity, and hence on its location[12–15]. Figure 1 illustrates how the Itô, Stratonovich, and isothermal conventions affect the stochastic step size in the presence of a viscosity gradient. A particle will exhibit no average drift in a viscosity gradient if it obeys Itô's calculus, since its steps will have the same size regardless of the direction. If it evolves according to the isothermal convention, it will drift toward lower viscosity as it takes larger average steps in that direction. From another perspective, the question of integration convention boils down to how one should generalize Fick's Law of diffusion for a concentration ρ of particles, $J = -D\nabla\rho(x)$, in cases where D varies in space[4]. The *Fokker-Planck* generalization, which corresponds to the Itô integration rule, puts the gradient operator outside the diffusivity and gives $J = -\nabla(D(x)\rho(x))$. This results in a contribution to the flux that depends explicitly on the diffusivity gradient, the term $-\rho(x)\nabla D(x)$. The *Fick* generalization, which corresponds to the isothermal integration rule, leaves the gradient operator inside the diffusivity and gives $J = -D(x)\nabla\rho(x)$. This results in no explicit dependence of the flux on the diffusivity gradient.

In our nanofluidic experiments, we measured a current of counterions flowing in the direction of decreasing viscosity (i.e., increasing diffusivity). This seemed difficult to square with the $-\rho\nabla D$ flux term in the Fick generalization (which points in the opposite direction) or the ∇D-independent flux of the Fokker-Planck generalization. It led one of us to initially believe he might have reversed the leads on the ammeter, or in some other way inverted the current. Instead, as we will show below, it is possible to find a flux without an explicitly ∇D-dependent term in the flux expression. The key to explaining the sustained currents we measured lies in the boundary conditions. Commonly, studies of inhomogeneous diffusion focus on some closed domain which particles cannot enter or leave[15–18]. Such closed boundary conditions require a flux-less steady state[13]. On the other hand, periodic boundary conditions, which better represent the ability of electrodes to absorb and release ions at distant locations, have no such restriction. Along related lines, Marchesoni showed theoretically how the viscosity-induced drift of particles under the isothermal convention could be harnessed to design a Maxwell demon that transmits information in a preferred direction between boundaries that act as sources and sinks of particles[19]. Also, De Haan and Slater used simulations to show that a viscosity gradient causes a polymer, starting halfway inside a nanopore, to escape preferentially on the low-viscosity side[20].

2 Simulation design

We studied diffusion in a viscosity gradient with a simple model for the motion of particles. The basis for our model was the work of Volpe and Wehr, which uses the stochastic differential equation[21],

$$dx_t = \sqrt{2D(x)}dW_t \equiv \sigma(x)dW_t, \tag{1}$$

where $dx_t = x_t - x_{t'}$ is the change in position between times t and t', D is the diffusivity, $dW_t = W_t - W_{t'}$ is a random variable with mean zero and variance $t - t'$. In these simulations, the continuous path of a particle is broken into discrete steps, x_n, occurring with a regular time interval Δt. It is convenient to use $\sigma(x) \equiv \sqrt{2D(x)}$, which represents the size of each random step. The discrete form of equation 1 is

$$\Delta x = x_{n+1} - x_n = \sigma(x)(\pm\sqrt{\Delta t}). \tag{2}$$

The random variable dW_t in equation 1 has been represented in equation 2 by a discrete random variable $\pm\sqrt{\Delta t}$ (where the $\pm$ represents the random choice), which has variance Δt. We set $\Delta t = 1$ and used a spatial domain 100 units wide. Typically, in simulations like this one, when a particle would pass through a boundary at $x = 0$ or $x = 100$, it is instead reflected back into the domain[21]. Figure 3a shows a diagram of a particle whose final position would have sent it past the boundary by a distance a. Instead, the particle is placed a distance a inside the domain. This rule is known as a *reflective* boundary condition[21].

For a system without a diffusivity gradient, the applica-

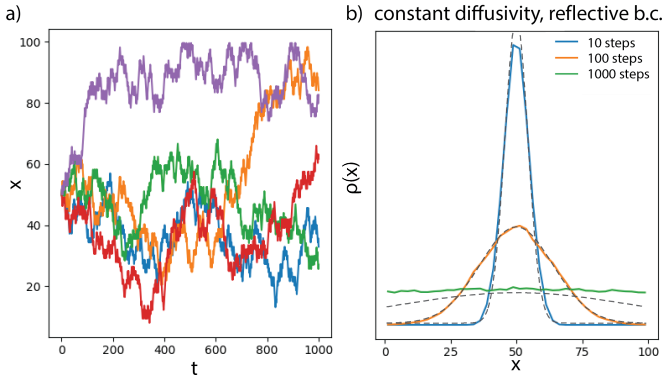

Fig. 2 Simulated diffusion of 10^5 particles with reflective boundary conditions and spatially-constant diffusivity. a) Five sample particle trajectories. b) The distribution of particles after 10, 100, and 1000 time steps. Dashed lines show theoretical expectation according to equation 3.

tion of equation 2 is uncomplicated. We simply generate a random choice, either $\sqrt{\Delta t}$ or $-\sqrt{\Delta t}$, multiply it by σ, add the result to x_n, and repeat. Figure 2a shows five sample trajectories for particles with $D = 1$. Particles are just as likely to go in either direction. The particles start tightly clustered but spread out over time. By 1000 steps, they look randomly distributed. The purple trajectory in Fig. 2a shows a particle bumping against the wall at $x = 100$. Figure 2b shows the distributions of 10^5 particles with uniform diffusivity $D = 1$ after 10, 100, and 1000 time steps. The particles were released from an initially Gaussian distribution centered at $x = 50$ with a standard deviation 1. The sharply peaked distribution spreads symmetrically about $x = 50$, relaxing to a half-max width of about 10 after 10 time steps and 35 after 100 steps. By step 1000, the distribution was nearly flat. We compared the simulated distributions with the analytic solution for point-source free diffusion: a Guassian function whose width increases with time,

$$\rho(x,t) = \frac{N}{\sqrt{4\pi Dt}} e^{-x^2/4Dt}, \tag{3}$$

where N is the number of particles. Our simulation matches equation 3 well after 10 and 100 steps, but shows an overabundance of particles everywhere after 1000 steps. This is because equation 3 is a solution for diffusion in free space, but our simulation will not let particles leave the domain.

Introducing a diffusivity gradient complicates the model in an important way. Each particle begins a step at a position x_n and ends at x_{n+1} so we have to choose where in that interval to evaluate function $\sigma(x)$; any location from x_n to x_{n+1} is equally valid. We could use the Itô convention, evaluating the diffusivity at the beginning of the step:

$$x_{n+1} = x_n \pm \sigma(x_n)\sqrt{\Delta t}. \tag{4}$$

We could use the Stratonovich convention, evaluating the diffusivity in the middle of the step:

$$x_{n+1} = x_n \pm \sigma\left(\frac{x_{n+1}+x_n}{2}\right)\sqrt{\Delta t}. \tag{5}$$

Finally, we could use the isothermal convention, evaluating it at the end:

$$x_{n+1} = x_n \pm \sigma(x_{n+1})\sqrt{\Delta t}. \tag{6}$$

The Itô convention, represented by equation 4, is the easiest to implement in a simulation because we know the current position of each particle and can straightforwardly computer the value of $\sigma(x_n)$. Equations 5 and 6 present an apparent catch-22. They require us to know where the particle will land to find the step size, but, of course, we must know the step size to compute where the particle will land. We will show how to find x_{n+1} in a self-consistent manner by first noting that equations 4, 5, and 6 can be expressed as special cases of a more general equation in which a continuous parameter α represents the choice of where to evaluate $\sigma(x)$,

$$x_{n+1} = x_n \pm \sigma(x_n + \alpha\Delta x)\sqrt{\Delta t}. \tag{7}$$

The parameter α runs from 0 to 1, and equations 4, 5, and 6 are special cases with $\alpha = 0$, $1/2$, and 1 respectively. We Taylor expand equation 7 to first order about the point x_n to find an equation for x_{n+1} based on x_n and the gradient in the diffusivity,

$$\sigma(x_n + \alpha\Delta x) \approx \sigma(x_n) + \alpha\frac{d\sigma(x)}{dx}\Delta x. \tag{8}$$

Substituting in equation 2 gives

$$\sigma(x_n + \alpha\Delta x) \approx \sigma(x_n) \pm \alpha\sigma(x_n)\frac{d\sigma(x_n)}{dx}\sqrt{\Delta t} \tag{9}$$

and applying to equation 7 gives a way to calculate x_{n+1} in terms of x_n for any value of α,

$$x_{n+1} = x_n + \alpha\sigma(x_n)\frac{d\sigma(x_n)}{dx}\delta t \pm \sigma(x_n)\sqrt{\delta t}. \tag{10}$$

In terms of $D(x)$, this would be,

$$x_{n+1} = x_n + \alpha\frac{dD(x_n)}{dx}\delta t \pm \sqrt{2D(x_n)\delta t}. \tag{11}$$

Consider a step subject to the isothermal rule as given by

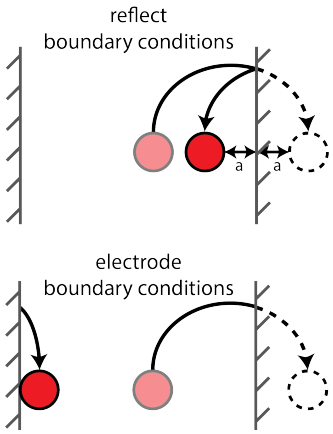

Fig. 3 a) A particle hopping into a reflective boundary condition. b) A particle hopping into a boundary condition designed to emulate an electrode.

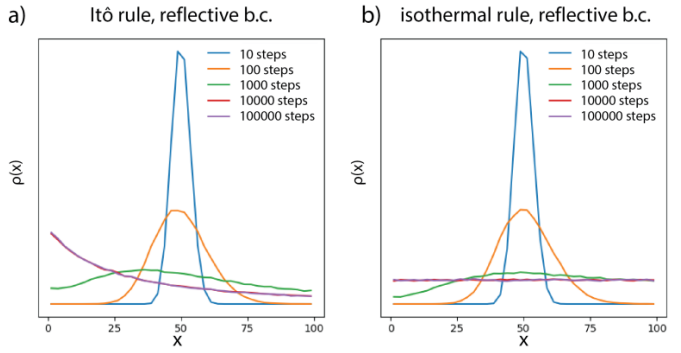

Fig. 4 Simulated diffusion of 10^5 particles with reflective boundary conditions using different integration conventions. Evolution of the particle distribution using a) the Itô convention and b) the isothermal convention.

equation 7 with $\alpha = 1$. The diffusive third term in equation 7 updates the position based on $\sigma(x_n)$, as prescribed by the Itô convention. By adding the second term, sometimes called the *spurious* or *noise-induced* drift, we recover the results of the isothermal convention[4,21,22]. In other words, a trajectory in the isothermal convention is equivalent to one in the Itô convention with an added drift term[21,22].

3 Results of simulations with diffusivity gradients

3.1 Using reflective boundary conditions

In their paper, Volpe and Wehr studied the Itô, Stratonovich, and isothermal integration conventions using simulations and demonstrated how this choice affects the steady-state particle distribution, finding a monotonically decreasing particle density when using the Itô convention, and a flat one when using the isothermal convention[21]. We set our simulation parameters to match those of Volpe and Wehr's, including $\sigma(x) = 0.2 + 0.02x$, a formula estimated from Fig. 4 of[21].Importantly, we used the same *reflective* boundary condition shown in figure 3 that Volpe and Wehr did. The simulation contains 10^5 particles with an initial Gaussian distribution with mean 50 and standard deviation 1, sampled at intervals up to 10^6 time steps, enough to reach the steady state.

Our results closely match those of Volpe and Wehr. Figure 4a shows the distribution of particles in a simulation of diffusion using the Itô convention. After 10 and 100 steps, the initial distributions widened and skewed slightly to the left. By $t = 10^3$, the tails of the distribution reached the boundaries, and the distribution is skewed noticeably left. It is clear the system has reached steady state by 10^4 steps because no further change is visible by 10^5 steps. Particles have piled up against the left boundary. After reaching the steady state, we measured no significant flux across $x = 50$.

Likewise, Fig. 4b shows diffusion under the $\alpha = 1$ or isothermal convention. The distributions look roughly Gaussian until 10^2 steps. After 10^3 steps, the distribution has reached the boundary at $x = 100$, but not the one at $x = 0$. By 10^4 steps, the system reached a steady state with a flat distribution and no significant flux through $x = 50$.

The absence of flux in these cases is not a surprise. In a closed container like the one simulated here, flux cannot exist anywhere in steady state. This constraint, along with spatial differences in hop length, allows us to understand the asymmetric steady state distribution resulting from the Itô rule in figure 4a, as well as the flat distribution resulting from the isothermal rule in figure 4b. Figure 5a shows, for an arbitrary test point x', the farthest points to the left and right from which particles are capable of hopping to or past x' for the Itô convention. The region on the right is always larger than that on the left because the diffusivity increases toward the right so hops originating from that direction are longer. Figure 5a also shows the equilibrium particle distribution, as calculated by our simulation and shown in figure 4a. The regions under the ρ curve shaded with orange and blue and are proportional to the number of particles that can possibly pass x' from the left and right respectively. Since particles jump left and right with equal probabilities in our model, the areas of these regions are proportional to the average number of particles that will cross x' in each direction in a given time step. Any difference in these areas indicates that a net flux will flow away from the larger region. The system must reach an equilibrium where the particle distribution always decreases toward the right in a way that compensates for the difference in hop length and brings the shaded areas into equality.

Figure 5b again shows the region to the left and right of an arbitrary point x' inside which particles are capable

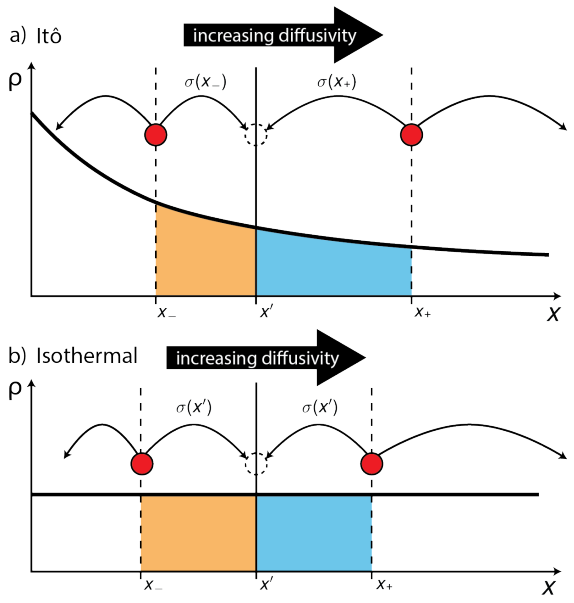

Fig. 5 Simulated equilibrium particle densities in the a) Itô convention and b) isothermal convention. Dotted lines show the farthest positions, x_+ and x_-, from which particles can cross a test point, x', from the left and right respectively. The areas of the shaded regions below the curve are proportional to the approximate number of particles that can cross x' from the left (orange) and the right (blue) in one step.

of hopping past x', but this time for the isothermal rule. The hop lengths are based on the hop's end position, so the sizes of these regions are equal. In this closed system, the flux must eventually reach zero everywhere. For the shaded regions to be equal for every choice of x', the equilibrium distribution must be flat, which is what we see in figure 4b. Equation 10 suggests another perspective from which to view the isothermal convention of stochastic motion. As hopping with hop-length determined by the starting position, with a superimposed drift proportional to the gradient in the diffusivity.

Which stochastic integration convention gives the correct physical description of ions in a liquid? The isothermal convention is strongly preferred on thermodynamic grounds: Only the isothermal convention gives a uniform particle distribution in a closed domain at thermal equilibrium, so it alone respects the Boltzmann distribution[13].

3.2 Using electrode boundary conditions

The reflective boundary conditions used above are a poor model for our experiments, where electrodes at either end of the mixing channel can absorb and release ions instead of reflecting them. When an ion in a nanochannel arrives at an electrode it can be absorbed and effectively re-emitted

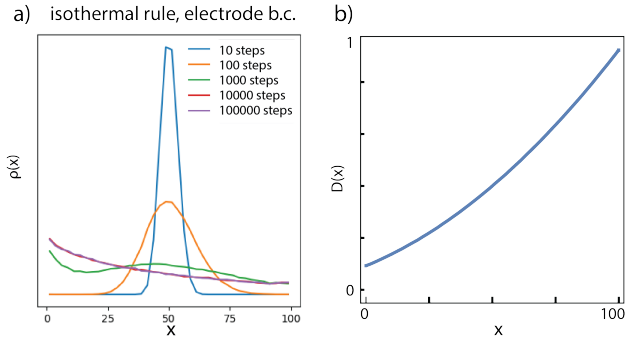

Fig. 6 Simulated diffusion of 10^5 particles with electrode boundary conditions using the isothermal convention. a) Evolution of the particle distribution. b) Diffusivity as a function of x.

at the opposite electrode. This wraps the domain into a circle and breaks the requirement that the flux be zero. We studied the following boundary condition as a toy model for electrodes: Any particle that would pass a boundary in the simulation is counted and moved to the opposite boundary. Figure 3b illustrates a particle that would hop past the boundary instead being placed inside the domain at the opposite boundary.

Figure 6a shows the evolution of the simulated particles distribution using the isothermal convention. This simulation was the same as the one in figure 4b, but with the electrode boundary conditions described above. Figure 6b shows the diffusivity function used in the simulation. By step 10^4, the system reached the steady state. This time, the distribution is not flat. The concentration is highest on the left and decreases monotonically to the right.

Figure 7a illustrates the regions in which particles can reach or pass x' in one step, along with the distribution of particles found in the isothermal experiment with electrode boundary conditions. The left shaded region under the curve is larger than the right shaded region, meaning that we expect net right-ward flux. In the steady state, this flux must be constant for every choice of x', including at the boundaries. This constraint determines the magnitude of the flux. Figure 7b shows the regions inside which particles can reach the boundaries at $L = 0$ and $L = 100$. The difference in the areas of these regions represents the flux through the boundary, which must be equal to the flux everywhere else in the steady state.

4 Comparison with experiment

Our simulations show the effects of the integration convention and boundary conditions, but how do they compare to our experiments? We performed simulations to qualitatively match our experiments. In those experiments, we varied the viscosity on both sides of our nanochannel,

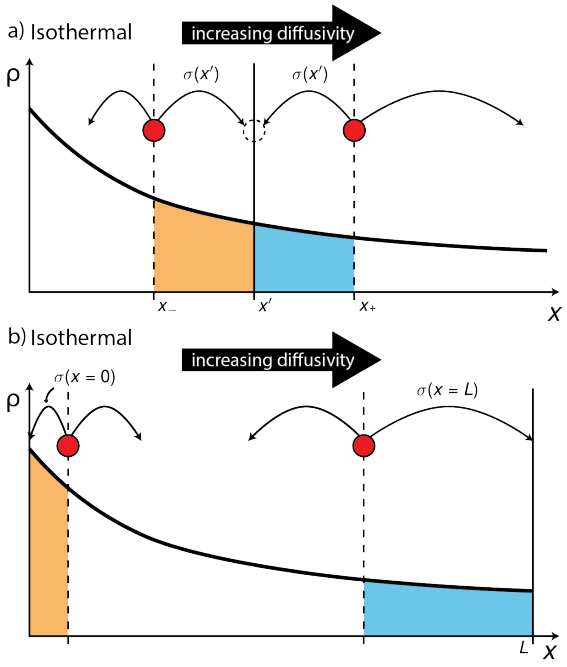

Fig. 7 Simulated equilibrium particle density in the isothermal convention with electrode boundary conditions. a) Dotted lines show farthest positions from which particles can reach or cross a test point, x', from the left and right. The areas of the shaded regions are proportional to the number of particles that can reach or cross x' from the left (orange) or right (blue) in one step. b) Dotted lines show the farthest positions from which particles can reach or cross the boundaries at $L = 0$ and $L = 100$. Area of the shaded regions is proportional the number of particles with a chance to hit the boundary at $x = 0$ (orange) or $x = 100$ (blue) in one step.

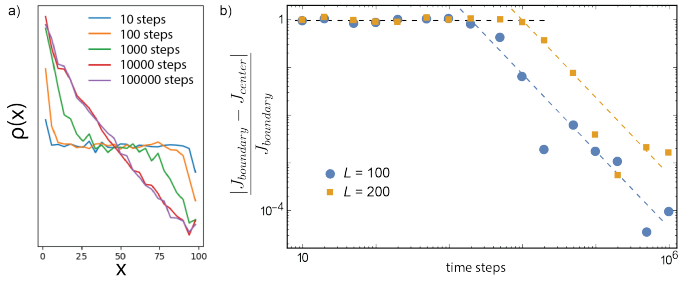

Fig. 8 a) The evolution of an initially flat particle distribution with the isothermal rule and electrode boundary conditions. b) The fractional absolute difference in flux at the center and at the boundaries for simulations with domain sizes of 100 and 200.

the length of our nanochannel, the pH of the solution, and the bulk salt concentration. In the simulations that follow, we tried to match the features of our experiments more closely; for example, accounting for a channel length L that could vary from 50 to 200 in units of micrometers. We only used the isothermal integration rule and electrode boundary conditions. In the simulations discussed above, we used linear functions for $\sigma(x)$ to match the conditions used by Volpe and Wehr[21]. In the simulations reported below, we used a linear diffusivity gradient to describe the inside of the nanochannel, where two different liquids would intermix. We also used a flat initial particle distribution to hasten the arrival at the steady state.

The result, we noticed, was that the simulator would initially register flux at the boundaries, but no flux at the center. After a relatively long delay, the flux at the center would catch up. Figure 8a shows the evolution of a flat particle distribution toward the steady state. The initially flat distribution at the midpoint of the channel explains the lack of flux there. The gradient in $\rho(x)$ seems to build in from the boundaries. Figure 8b shows the absolute difference between the center and boundary fluxes (as a fraction of the boundary flux) for a range of times as the system approaches the steady state. Two different simulations, with domain sizes of 100 and 200, are compared. Initially, the fractional flux difference is 1, because all of the flux is at the boundary. At about step 2000 for the $L = 100$ simulation and step 10 000 for the $L = 200$ simulation, that difference starts to drop. Eventually, the difference becomes negligible as the fluxes converge to the same number and the system enters the steady state. We used analysis like this to guide the lengths of our simulations.

To compare with our viscosity-varying experiments, we performed simulations with a variety of diffusivity profiles. We simulated 10^5 particles according to the isothermal rule for 2×10^5 times steps, counting flux for the last 5×10^4 steps. After the system reached equilibrium, we started

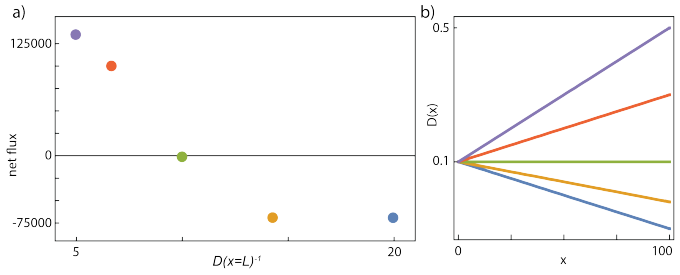

Fig. 9 Flux in simulations with several diffusivity ratios using the isothermal rule and electrode boundary conditions. a) Dependence of flux on $D(x=L)^{-1}$. b) Diffusivity profiles, color coded to match points in (a).

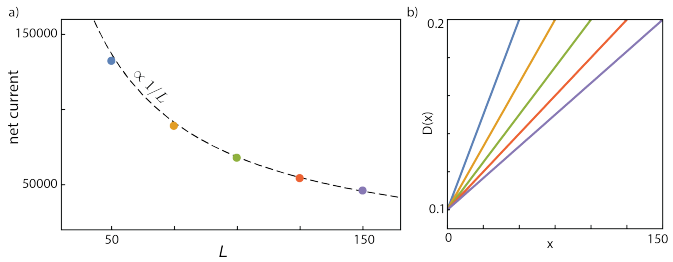

Fig. 10 Flux in simulations with several domain lengths using the isothermal rule and electrode boundary conditions. a) Dependence of flux on L. b) Diffusivity profiles, color coded to match points in (a).

counting the flux at the boundaries and at $x = L/2$.

Figure 9a shows the simulated flux as a function of the inverse diffusivity at $x = L$ with the viscosity at $x = 0$ fixed at $\eta(x = 0) = 10$. Figure 9b shows the diffusivity profiles used for each data point. We have used inverse diffusivity as the independent variable here to represent viscosity and make the plot easier to compare with our experimental observations. The agreement is clear: ions flow toward lower viscosity. We also note that the curve flattens out at higher values of D^{-1}.

Figure 10a shows the simulated flux as a function of the simulation domain size. The particle number density, N/L, and diffusivities at the boundaries, $D(x = 0)$ and $D(x = L)$, were kept constant. Figure 10b shows the diffusivity gradients used, where the color corresponds to the color of the data points in figure 10a. As the domain gets longer, the gradient decreases and so does the drift speed. The dotted line in figure 10a shows the expected flux dependence, $1/L$. This matches the linear dependence of the current on the viscosity gradient observed experimentally.

5 Conclusions

Simulations have illuminated the mechanisms of diffusive ion transport in a gradient of liquid viscosity. The boundary conditions turn out to be essential. The reflective boundary conditions that simulate a closed container make it impossible for a steady-state flux to exist. However, boundary conditions which represent the ability of electrodes to absorb and release ions allow a steady-state flux. Using the isothermal convention and electrode boundary conditions, particles exhibit a noise-induced drift in the direction of lower viscosity that produces a flux, and this flux has the important features of ionic currents measured in our nanochannels. Finally, we note that a viscosity-driven current of counterions does not violate any thermodynamic principle. We experimentally maintain the viscosity gradient in our nanochannels by replenishing the liquids at either end of the nanochannel, and this holds out of equilibrium. As the liquids intermix, the free energy of mixing is available to drive a steady current.

Conflicts of interest

There are no conflicts of interest to declare.

Acknowledgements

This material is based upon work supported by the National Science Foundation under Grant No. 1904511 and by Oxford Nanopore Technologies, Ltd.

Notes and references

1 A. Einstein, *Annalen der physik*, 1905, **17**, 549–560.
2 M. Von Smoluchowski, *Annalen der physik*, 1906, **326**, 756–780.
3 S. Chandrasekhar, *Reviews of modern physics*, 1943, **15**, 1.
4 N. G. Van Kampen and W. P. Reinhardt, *Stochastic processes in physics and chemistry*, 1983.
5 K. Itô, *Proceedings of the Imperial Academy*, 1944, **20**, 519–524.
6 R. Jarrow, P. Protter *et al.*, *A festschrift for Herman Rubin*, Institute of Mathematical Statistics, 2004, pp. 75–91.
7 R. Stratonovich, *Vestnik Mosk. Univ., Ser. I: Mat. Mekh.*, 1964, **1**, 3–12.
8 R. Stratonovich, *SIAM Journal on Control*, 1966, **4**, 362–371.
9 D. L. Fisk, *Quasi-martingales and stochastic integrals*, Michigan state univ east lansing technical report, 1963.
10 P. Hanggi, *a* { *a*, volume=1, pages=a2, year=1980.
11 P. Hänggi and H. Thomas, *Physics Reports*, 1982, **88**, 207–319.
12 N. Van Kampen, *Journal of physics and chemistry of solids*, 1988, **49**, 673–677.
13 A. W. Lau and T. C. Lubensky, *Physical Review E*, 2007, **76**, 011123.

14 I. Sokolov, *Chemical Physics*, 2010, **375**, 359–363.
15 G. Volpe, L. Helden, T. Brettschneider, J. Wehr and C. Bechinger, *Physical review letters*, 2010, **104**, 170602.
16 E. R. Dufresne, D. Altman and D. G. Grier, *EPL (Europhysics Letters)*, 2001, **53**, 264.
17 J. Happel and H. Brenner, *Low Reynolds number hydrodynamics: with special applications to particulate media*, Springer Science & Business Media, 2012, vol. 1.
18 E. Kätelhön, S. V. Sokolov and R. G. Compton, *Sensors and Actuators B: Chemical*, 2016, **234**, 420–425.
19 F. Marchesoni, *Materials*, 2013, **6**, 3598–3609.
20 H. W. de Haan and G. W. Slater, *Physical Review E*, 2013, **87**, 042604.
21 G. Volpe and J. Wehr, *Reports on Progress in Physics*, 2016, **79**, 053901.
22 H. W. de Haan, M. V. Chubynsky and G. W. Slater, *arXiv preprint arXiv:1208.5081*, 2012.